Batiza, R., Storms, M.A., and Allan, J.F. (Eds.), 1995
Proceedings of the Ocean Drilling Program, Scientific Results, Vol. 142

6. 1-ATM MELTING STUDY OF A LEG 142 BASALT: IMPLICATIONS FOR FRACTIONATION PROCESSES BENEATH THE EAST PACIFIC RISE AT 9°30′N[1]

James G. Brophy[2]

ABSTRACT

A series of 1-atm phase equilibrium experiments was conducted on a moderately evolved normal mid-ocean ridge basalt sampled during drilling of the East Pacific Rise (EPR) ridge crest at 9°30′N. The compositions of olivine-plagioclase-clinopyroxene-saturated liquids are used to define the position of a 1-atm cotectic boundary curve on an olivine-clinopyroxene-quartz pseudo-ternary projection diagram. Comparison of this boundary curve with the projected positions of natural lavas erupted along this same portion of the EPR suggests a fractional crystallization origin at somewhat elevated pressures. The actual fractionation pressure is estimated at 1.9 ± 0.3 kb based on (1) a comparison of observed and predicted CaO-MgO variation slopes as a function of pressure, and (2) an estimation of the pressure at which the liquidus of the starting basalt composition is multiply saturated with olivine, plagioclase, and clinopyroxene. The above pressure estimate places the location of fractional crystallization within the lower crust and well beneath the axial magma chamber that exists about 1.5 km beneath the seafloor. Given that little to no fractional crystallization occurs within the axial magma chamber, it is suggested that fractional crystallization occurs during upward melt migration as rising melts pass through and interact with solid and partially crystalline material in the roots of the magmatic system

INTRODUCTION

Recent geologic, petrologic, and geophysical studies of both fast- and slow-spreading mid-ocean ridges have led to a modern view of mid-ocean ridge magmatic plumbing systems that is quite different than the time-honored notion of a large (several kilometer thick), long lived, continuously replenished magma chamber beneath the entire length of the ridge axis (e.g., Bryan and Moore, 1977; Pallister and Hopson, 1981). Instead, it is now believed that the region beneath the ridge crest consists largely of a crystal-rich mush that grades downward and outward through increasingly crystalline material into solid gabbro and/or mantle material (e.g., Sinton and Detrick, 1992; Fig. 1). Beneath fast-spreading ridge systems such as the East Pacific Rise (EPR), this mush zone is commonly, though not necessarily, capped by a thin, sill-like axial magma chamber that lies approximately 1.5 km beneath the seafloor at a pressure of about 1 kb. In contrast, evidence for similar magma chambers beneath slow-spreading ridges such as the Mid-Atlantic Ridge (MAR) is absent and the entire magmatic plumbing system is believed to consist of mushy rocks of varying degrees of crystallinity. An important aspect of this new view of mid-ocean ridge magmatic plumbing systems is that it has forced a reevaluation of how and where fractional crystallization and other differentiation processes operate beneath spreading centers in general, and slow- and fast-spreading ridge systems in particular.

A comparison of erupted lava compositions from slow- and fast-spreading ridge systems has shown that fast-spreading ridges are characterized by lavas that are more evolved than those erupted along slow-spreading ridges (e.g., Sinton and Detrick, 1992). This difference in erupted lava compositions must be a reflection of differences in the nature of the magmatic plumbing system at depth, and may or may not reflect differences in the depth of fractional crystallization as

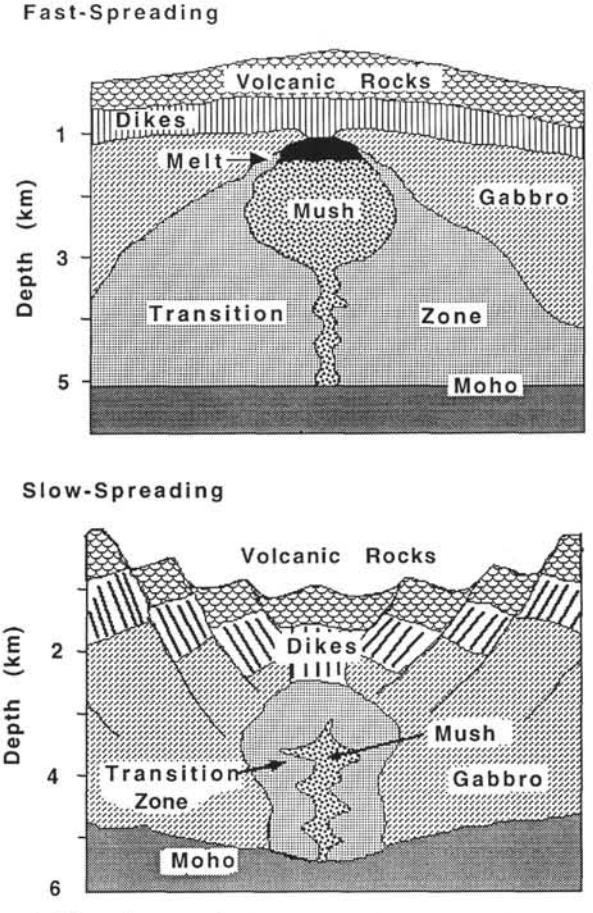

Figure 1. Schematic cross-axis diagrams showing an interpretive model of magmatic plumbing systems beneath fast- and slow-spreading mid-ocean ridge systems (after Sinton and Detrick, 1992).

[1]Batiza, R., Storms, M.A., and Allan, J.F. (Eds.), 1995. *Proc. ODP, Sci. Results,* 142: College Station, TX (Ocean Drilling Program).

[2]Department of Geological Sciences, Indiana University, Bloomington, IN 47405, U.S.A.

well as the nature of the actual fractionation processes themselves. Recent experimental phase equilibrium studies of selected basalt lavas from slow-spreading ridge systems (e.g., Tormey et al., 1987; Grove et al., 1990, 1992) have suggested that fractionation occurs over a pressure range of 3 to 6 kb, which places much, if not all of the fractionation within the upper mantle. Given the apparent lack of any long-lived magma chamber at such depths, it may be inferred that fractional crystallization occurs within individual bodies of magma as they traverse the upper mantle on their way to the surface (e.g., Grove et al., 1992). In contrast, the greater degrees of compositional evolution along fast-spreading ridge systems, coupled with the common presence of actual magma chambers, have led many workers to suggest that fractionation processes within the low-pressure axial magma chamber ($P \approx 1$ kb) may still play an important role in determining the final composition of erupted lavas. The purpose of this study is to address the latter possibility.

One way of addressing this important question is to determine the fractionation pressure of a typical suite of fractionation-related lavas erupted along a fast-spreading mid-ocean ridge. One of the best studied portions of a fast-spreading ridge system is the EPR between 9° and 12°N (e.g., Langmuir et al., 1986; Thompson et al., 1989; Reynolds et al., 1992; Batiza and Niu, 1992). This study describes the results of low-pressure (1-atm) phase equilibrium experiments conducted on a moderately evolved normal mid-ocean ridge basalt (N-MORB) recovered during Ocean Drilling Program Leg 142 at the fast-spreading EPR ridge crest at 9°30′N. The experiments quantify the 1-atm liquid line of descent as well as the phase appearance sequence and phase proportions expected from low-pressure crystallization of N-MORB magma beneath this segment of the EPR. Batiza and Niu (1992) have presented a large data set containing well over a hundred analyses of erupted lavas along this same segment of the EPR and have concluded that the compositional variation among lavas is best explained by fractional crystallization. The experimental data derived from this study have been compared with the observed compositional characteristics of these fractionation-related lavas to assess the pressure at which fractional crystallization occurred. Based on these results, the role of fractionation processes within the low-pressure axial magma chamber as well as the actual nature of the fractionation processes themselves have been addressed.

EXPERIMENTAL AND ANALYTICAL METHODS

Drilling at Hole 864A retrieved rock fragments from two N-MORB units (Unit I and Unit II). Each unit is believed to represent a single eruptive event (Batiza et al., this volume). The starting composition used in this study is derived from several fragments of the Unit I basalt. Unit I is a moderately evolved N-MORB with 7.3 wt% MgO (Table 1), which places it almost exactly in the middle of the observed MgO range of lavas erupted along this segment of the EPR (Batiza and Niu, 1992). Unit I rock fragments are all very sparsely phyric with total phenocryst contents of only 1–2 volume percent. Groundmass textures range from glassy to variolitic to microcrystalline. Plagioclase is the sole phenocryst phase.

Individual glassy (glass + 1%–2% plagioclase phenocrysts) and microcrystalline (groundmass olivine, plagioclase, clinopyroxene, opaque minerals + 1%–2% plagioclase phenocrysts) powders were created by hand-picking glassy and microcrystalline rock fragments from Samples 142-864A-1M-3, 0–150 cm, and 142-864A-1M-5, 0–150 cm, and then reducing them to fine powder in a SPEX Tungsten-Carbide shatter box for approximately 8 min. Exactly 90 g of the glassy powder and 10 g of the crystalline powder were then placed in a SPEX Tungsten-Carbide Ball Mill (minus the balls) and shaken for approximately 10 minutes. The final result was a starting material that was largely glass but with a small amount of crystalline seed material evenly distributed throughout. Table 1 lists chemical analyses of the starting composition used in this study.

Table 1. Analyses of Unit I Sample 142-864A-1M-3, 0–150 cm, starting material.

	Unit 1 (avg)[a]	Unit 1 glassy rock fragment 142-864A-1M-3, 0–35 cm[a]	Unit 1 crystalline rock fragment 142-864A-1M-3, 100–150 cm[a]	1-atm fused glass 142-864A-1M[b]
SiO_2	49.91	49.8	49.96	50.65
TiO_2	1.64	1.64	1.66	1.73
Al_2O_3	14.3	14.28	14.27	14.23
FeO*	10.55	10.54	10.62	10.1
MnO	0.2	0.2	0.2	0.2
MgO	7.3	7.21	7.35	7.55
CaO	11.72	11.68	11.7	11.8
Na_2O	2.55	2.59	2.53	2.83
K_2O	0.14	0.13	0.13	0.13
P_2O_5	0.11	0.1	0.1	0.13
Total	98.42	98.17	98.52	99.35

Note: FeO* = total iron.
[a]Shipboard X-ray fluorescence analysis.
[b]Microprobe analysis.

All experiments were carried out at 1-atm in the University of Oregon experimental petrology laboratory using techniques routinely employed there. A small amount of the starting powder (approximately 0.15 to 0.2 grams) was mixed with polyvinyl alcohol to create a viscous slurry which was then applied to a thin (0.004-inch diameter) platinum wire and allowed to dry. The sample was placed in the isothermal zone of a Deltech DT31VT quenching furnace with a CO_2-H_2 gas atmosphere maintained at the quartz-fayalite-magnetite buffer. At the end of the run, the sample was quenched in a water bath. Oxygen fugacity was monitored using a zirconia-based solid electrolyte cell calibrated at the Fe-FeO buffer. Temperature was monitored using a Pt-10Rh thermocouple calibrated against the melting point of Au. Experimental conditions and phase appearance temperatures are reported in Table 2 and shown in Figure 2. Based upon subsequent mass balance calculations, Fe loss to the platinum wire holder was minimal. However, Na_2O loss was found to be significant in many of the lower temperature and/or longer duration runs (Table 2). All glass analyses used in subsequent data analysis have been corrected for Na_2O loss.

All run products with the exception of one (142-QFM-4, 1185°C) were mounted in epoxy, polished to a smooth finish, and then examined by standard reflected light petrography, electron back-scatter imaging, and wave-length dispersive microprobe analysis. Microprobe analyses of plagioclase were performed on a four-spectrometer CAMECA SX-50 microprobe located at Indiana University while all glass, olivine, and clinopyroxene analyses were performed on a similar instrument located at the University of Oregon. Standard operating conditions included a 15 kV accelerating voltage, a 10 nA sample current for glass, a 15 nA current for plagioclase, and a 20 nA current for olivine and clinopyroxene. Back-scatter electron imaging indicated little to no compositional zonation within individual crystals in high-temperature, low-crystallinity experiments. However, crystalline phases in the lower temperature and higher crystallinity runs displayed mild to significant zonation. To reduce the likelihood of measuring and reporting mineral and glass compositions that are not in equilibrium with one another, only mineral rims were analyzed. All mineral and glass analyses are summarized in Table 3.

EXPERIMENTAL RESULTS

One-atmosphere Liquid Line of Descent: Evidence for Elevated-Pressure Fractional Crystallization beneath the EPR

The results of the 1-atm melting experiments are summarized in Figure 2. The first phase to crystallize from the liquid is olivine

Table 2. Run conditions and phase assemblages.

Run number	Temperature (°C)	Time (hr)	log (fO_2)	Assemblage	Proportions	Estimated Na_2O loss (wt%)	Na_2O loss (relative %)
142-QFM-3	1190	24.5	–8.42	gl	100	0	0
142-QFM-4[a]	1185	24	–8.48	gl	100	0	0
142-QFM-1	1180	24	–8.53	gl,ol	100:tr	0	0
142-QFM-8	1175	24.5	–8.59	gl, pl, ol	98:1:1	0.15	5.26
142-QFM-2	1170	25	–8.65	gl, pl, ol	97:2:1	0	0
142-QFM-9	1165	24	–8.71	gl, pl, ol, cpx	90:6:3:1	0	0
142-QFM-14	1160	24	–8.77	gl, pl, ol, cpx	82:9:3:6	0.22	7.72
142-QFM-10	1155	24	–8.83	gl, pl, ol, cpx	75:14:3:8	0.21	7.37
142-QFM-6	1150	24	–8.89	gl, pl, ol, cpx	73:15:4:8	0.22	7.72
142-QFM-11	1145	47	–8.95	gl, pl, ol, cpx	69:16:4:11	0.26	9.12
142-QFM-7	1140	25	–9.01	gl, pl, ol, cpx	61:20:5:14	0.29	10.18
142-QFM-12	1135	46	–9.07	gl, pl, ol, cpx	60:21:4:15	0.29	10.18

Notes: gl = glass; pl = plagioclase; ol = olivine; cpx = clinopyroxene (augite); tr = trace. Phase proportions calculated using unweighted materials balance.
[a]Sample crushed and observed under oil. No microprobe analysis performed.

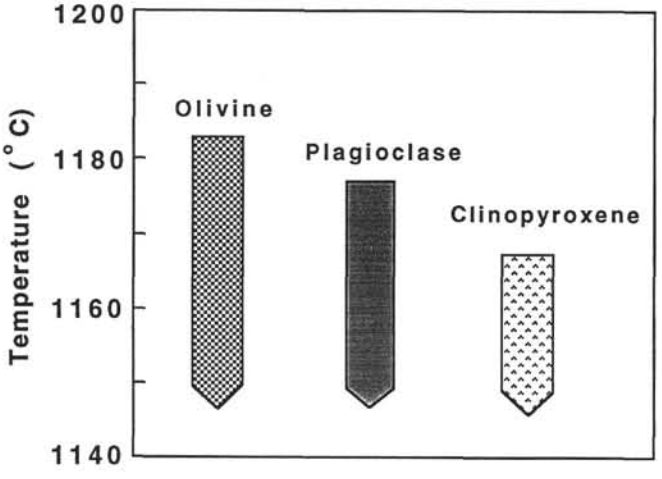

Figure 2. Experimentally determined sequence of appearance of crystalline phases.

(1182.5°± 2.5°C) followed by plagioclase (1177.5 ± 2.5°C) and then augite (1167.5°± 2.5°C). Replicate experiments over this temperature range have substantiated these crystallization temperatures. Both low-Ca pyroxene (orthopyroxene or pigeonite) and Fe-oxide are absent within the temperature range considered here, although exploratory experiments at much lower temperatures (1110° and 1120°) indicate that both phases eventually crystallize.

Figure 3 is a composite MgO-variation diagram with plots of the initial basalt starting composition (microprobe analysis of fused glass, Table 1), all experimentally determined liquid compositions, and 139 microprobe analyses of natural basalt glasses collected from along this section of the EPR (Batiza and Niu, 1992). The natural glass analyses are from essentially aphyric lavas and are thus believed to represent lava compositions that in turn represent preserved liquid compositions. The lavas range from 8.4 to 6.2 wt% MgO and define very tight, systematic variations for each oxide. The experimental liquids range from 7.6 to 5.6 wt% MgO. In general, the absolute abundances and slopes of individual oxide trends defined by the experimental liquids coincide with those defined by lavas. This strongly supports the fractional crystallization origin for the EPR lavas suggested by Batiza and Niu (1992). In detail, however, some subtle differences exist between the experimental and natural lava data, particularly with regard to Al_2O_3 and CaO. First, the variation in lava Al_2O_3 parallels that of the experimental liquids, but abundances in the lavas are systematically shifted to higher values. Second, the slope of the CaO variation is less steep than that defined by the experimental liquids, particularly those that are olivine-plagioclase-augite-saturated. These differences imply that other conditions (e.g., higher pressure fractionation) and/or processes (e.g., mixing, assimilation) must have been involved in generating the range of erupted lava compositions along this section of the EPR.

Estimating the Pressure of Fractional Crystallization

Numerous studies have emphasized the usefulness of pseudo-ternary phase diagrams for discerning the operation of various differentiation processes in the generation of MORB lavas (e.g., Walker et al., 1979; Grove and Bryan, 1983; Tormey et al., 1987; Thompson et al., 1989, Grove et al., 1992). Figure 4 shows the olivine-clinopyroxene-quartz pseudo-ternary of Walker et al. (1979) with projected compositions of all olivine-plagioclase-clinopyroxene-saturated experimental liquids from this study. The seven experimental liquids define a tight, linear array that trends towards the quartz apex of the diagram. High-temperature liquids project towards the quartz-poor end of the array whereas lower temperature liquids project toward the quartz-rich end. Together, the projected liquid compositions define a portion of a 1-atm olivine-plagioclase-clinopyroxene-liquid cotectic boundary curve that is appropriate for application to the lavas erupted within this segment of the EPR. To emphasize the importance of this, rather than some other pseudo-ternary diagram for use with the EPR suite of lavas under consideration, Figure 5 compares the cotectic boundary curve generated from the present EPR basalt starting composition with similar cotectic boundary curves generated from mid-Atlantic Ridge basalt starting compositions (Walker et al., 1979; Grove and Bryan, 1983; Tormey et al., 1987). The projected location and trend of the multiply-saturated boundary curve from this study is similar to that determined by Tormey et al. (1987) but is quite different from those determined by Walker et al. (1979) and Grove and Bryan (1983). Clearly, the initial basalt starting composition exerts a strong control on the resultant experimental liquid line of descent. Therefore, as pointed out already by Tormey et al. (1987), for assessing the conditions of differentiation of a given lava suite it is crucial that one use a phase diagram generated from a starting composition that is genetically related to the lavas under investigation.

In Figure 6, the 1-atm cotectic boundary curve from Figure 4 is compared with the projected positions of the EPR lava compositions reported by Batiza and Niu (1992). The lavas define a diffuse, linear array roughly parallel to the experimentally determined boundary curve, but slightly offset to the olivine-rich side of the 1-atm cotectic boundary curve. Several studies have shown that increased pressure displaces the boundary curve toward the olivine apex of this particular pseudo-ternary diagram (e.g., Stolper, 1980; Grove and Baker, 1983; Grove et al., 1992). Thus, the projected location of the EPR lavas implies that fractional crystallization occurred at somewhat elevated pressures.

Table 3. Glass and mineral compositions.

Run number	Temperature (°C)	Phase	(*n*)	SiO_2	TiO_2	Al_2O_3	FeO	MnO	MgO	CaO	Na_2O	K_2O	P_2O_5	Total
142-QFM-3	1190	gl	9	50.65 (0.14)	1.73 (0.06)	14.23 (0.06)	10.10 (0.11)	0.20 (0.02)	7.55 (0.05)	11.80 (0.04)	2.83 (0.03)	0.13 (0.01)	0.13 (0.02)	99.35 (0.24)
142-QFM-1	1180	gl	10	50.61 (0.09)	1.67 (0.04)	14.38 (0.04)	10.22 (0.06)	0.20 (0.02)	7.49 (0.03)	11.68 (0.04)	2.84 (0.02)	0.13 (0.01)	0.13 (0.02)	99.34 (0.14)
		ol	1	38.38 (0.00)			16.09 (0.00)	0.27 (0.00)	43.01 (0.00)	0.40 (0.00)				98.59 (0.00)
142-QFM-8	1175	gl	9	50.39 (0.09)	1.80 (0.05)	14.45 (0.06)	10.45 (0.09)	0.18 (0.01)	7.17 (0.02)	11.79 (0.02)	2.71 (0.03)	0.14 (0.01)	0.18 (0.02)	99.25 (0.13)
		pl	7	50.36 (0.17)		31.35 (0.17)	0.77 (0.03)			15.02 (0.08)	2.81 (0.03)	0.11 (0.01)		100.42 (0.13)
		ol	4	38.54 (0.14)			17.47 (0.06)	0.26 (0.01)	42.41 (0.05)	0.41 (0.02)				99.09 (0.18)
142-QFM-2	1170	gl	10	50.25 (0.17)	1.73 (0.05)	14.28 (0.06)	10.23 (0.08)	0.17 (0.01)	7.24 (0.03)	11.81 (0.03)	2.88 (0.02)	0.15 (0.01)	0.16 (0.03)	98.90 (0.25)
		pl	6	50.81 (0.21)		30.69 (0.16)	0.89 (0.02)			14.66 (0.09)	2.97 (0.03)	0.05 (0.01)		100.07 (0.11)
		ol	5	38.90 (0.06)			16.79 (0.19)	0.27 (0.01)	42.22 (0.08)	0.41 (0.02)				98.60 (0.17)
142-QFM-9	1165	gl	9	50.47 (0.14)	1.97 (0.08)	13.66 (0.06)	10.85 (0.13)	0.22 (0.02)	6.59 (0.06)	11.71 (0.05)	2.70 (0.02)	0.16 (0.01)	0.18 (0.01)	98.51 (0.11)
		pl	7	51.41 (0.09)		30.83 (0.09)	0.73 (0.03)			14.26 (0.07)	3.13 (0.02)	0.05 (0.01)		100.40 (0.12)
		ol	2	38.32 (0.11)			18.37 (0.17)	0.24 (0.01)	41.10 (0.03)	0.50 (0.02)				98.52 (0.01)
		cpx	4	53.23 (0.6)	0.74 (0.07)	2.53 (0.42)	6.55 (0.39)	0.16 (0.03)	17.42 (0.21)	19.33 (0.64)	0.22 (0.01)			100.18 (0.63)
142-QFM-14	1160	gl	10	50.87 (0.15)	1.85 (0.09)	13.87 (0.10)	11.12 (0.17)	0.17 (0.01)	6.52 (0.08)	11.46 (0.09)	2.81 (0.04)	0.16 (0.01)	0.21 (0.01)	99.03 (0.17)
		pl	10	50.60 (0.19)		30.49 (0.13)	0.84 (0.05)			13.79 (0.04)	3.32 (0.02)	0.04 (0.01)		99.07 (0.20)
		ol	6	37.65 (0.18)			21.14 (0.19)	0.33 (0.01)	39.23 (0.18)	0.46 (0.01)				98.81 (0.18)
		cpx	6	53.03 (0.21)	0.67 (0.02)	2.33 (0.16)	6.96 (0.14)	0.20 (0.02)	17.32 (0.19)	19.09 (0.28)	0.19 (0.01)			99.87 (0.23)
142-QFM-10	1155	gl	10	50.65 (0.12)	2.17 (0.08)	13.56 (0.06)	11.77 (0.16)	0.24 (0.01)	6.44 (0.06)	11.30 (0.05)	2.89 (0.04)	0.17 (0.01)	0.23 (0.02)	99.40 (0.14)
		pl	14	52.59 (0.26)		29.69 (0.23)	0.99 (0.05)			13.45 (0.10)	3.54 (0.05)	0.04 (0.01)		100.29 (0.19)
		ol	10	37.97 (0.09)			19.85 (0.26)	0.30 (0.01)	40.34 (0.23)	0.46 (0.02)				98.91 (0.13)
		cpx	5	52.53 (0.45)	0.91 (0.14)	3.10 (0.38)	7.66 (0.19)	0.19 (0.01)	16.85 (0.17)	19.07 (0.17)	0.24 (0.01)			100.55 (0.16)
142-QFM-6	1150	gl	6	50.15 (0.17)	2.10 (0.10)	13.37 (0.14)	11.71 (0.18)	0.23 (0.01)	6.27 (0.14)	11.20 (0.10)	2.87 (0.04)	0.17 (0.01)	0.17 (0.01)	98.24 (0.27)
		pl	6	51.89 (0.13)		30.37 (0.12)	0.88 (0.04)			13.77 (0.09)	3.33 (0.03)	0.04 (0.01)		100.29 (0.15)
		ol	1	38.17 (0.00)			20.13 (0.00)	0.27 (0.00)	39.18 (0.00)	0.61 (0.00)				98.36 (0.00)
		cpx	2	51.80 (0.47)	0.81 (0.09)	2.68 (0.11)	8.52 (0.56)	0.23 (0.01)	17.23 (0.50)	18.71 (0.16)	0.20 (0.01)			100.37 (0.20)
142-QFM-11	1145	gl	11	50.77 (0.20)	2.43 (0.08)	13.16 (0.08)	11.98 (0.22)	0.26 (0.01)	6.07 (0.06)	10.83 (0.05)	2.85 (0.02)	0.19 (0.01)	0.24 (0.02)	98.80 (0.15)
		pl	14	51.85 (0.24)		30.08 (0.10)	0.85 (0.03)			13.37 (0.08)	3.50 (0.03)	0.03 (0.01)		99.67 (0.25)
		ol	5	37.66 (0.11)			21.45 (0.13)	0.37 (0.01)	38.71 (0.21)	0.53 (0.03)				98.72 (0.14)
		cpx	5	53.25 (0.19)	0.67 (0.07)	2.17 (0.32)	7.52 (0.27)	0.21 (0.01)	17.10 (0.19)	18.84 (0.17)	0.24 (0.02)			99.99 (0.31)
142-QFM-7	1140	gl	7	50.22 (0.14)	2.55 (0.10)	13.08 (0.10)	12.49 (0.10)	0.25 (0.02)	5.72 (0.04)	10.72 (0.08)	2.92 (0.06)	0.19 (0.01)	0.22 (0.01)	98.38 (0.26)
		pl	8	51.53 (0.20)		29.86 (0.18)	0.95 (0.07)			13.21 (0.09)	3.56 (0.06)	0.04 (0.01)		99.14 (0.17)
		ol	4	37.31 (0.15)			23.46 (0.28)	0.37 (0.02)	37.07 (0.18)	0.49 (0.02)				98.69 (0.14)
		cpx	5	51.89 (0.52)	0.99 (0.10)	3.87 (0.52)	8.53 (0.19)	0.23 (0.02)	15.72 (0.34)	18.45 (0.24)	0.27 (0.03)			100.07 (0.10)
142-QFM-12	1135	gl	12	50.78 (0.07)	2.72 (0.10)	12.87 (0.07)	12.61 (0.14)	0.25 (0.01)	5.69 (0.04)	10.43 (0.05)	2.89 (0.02)	0.22 (0.01)	0.25 (0.01)	98.70 (0.11)
		pl	9	52.43 (0.09)		29.46 (0.12)	0.89 (0.07)			12.77 (0.07)	3.76 (0.02)	0.04 (0.01)		99.35 (0.12)
		ol	4	37.45 (0.08)			23.75 (0.30)	0.38 (0.02)	36.74 (0.12)	0.55 (0.02)				98.88 (0.27)
		cpx	7	52.32 (0.50)	0.90 (0.14)	2.88 (0.47)	8.32 (0.21)	0.22 (0.02)	16.18 (0.28)	18.60 (0.24)	0.24 (0.02)			99.87 (0.16)

Notes: gl = glass; pl = plagioclase; ol = olivine; cpx = clinopyroxene (augite). Values in parentheses represent the 2-sigma standard deviation of the mean.

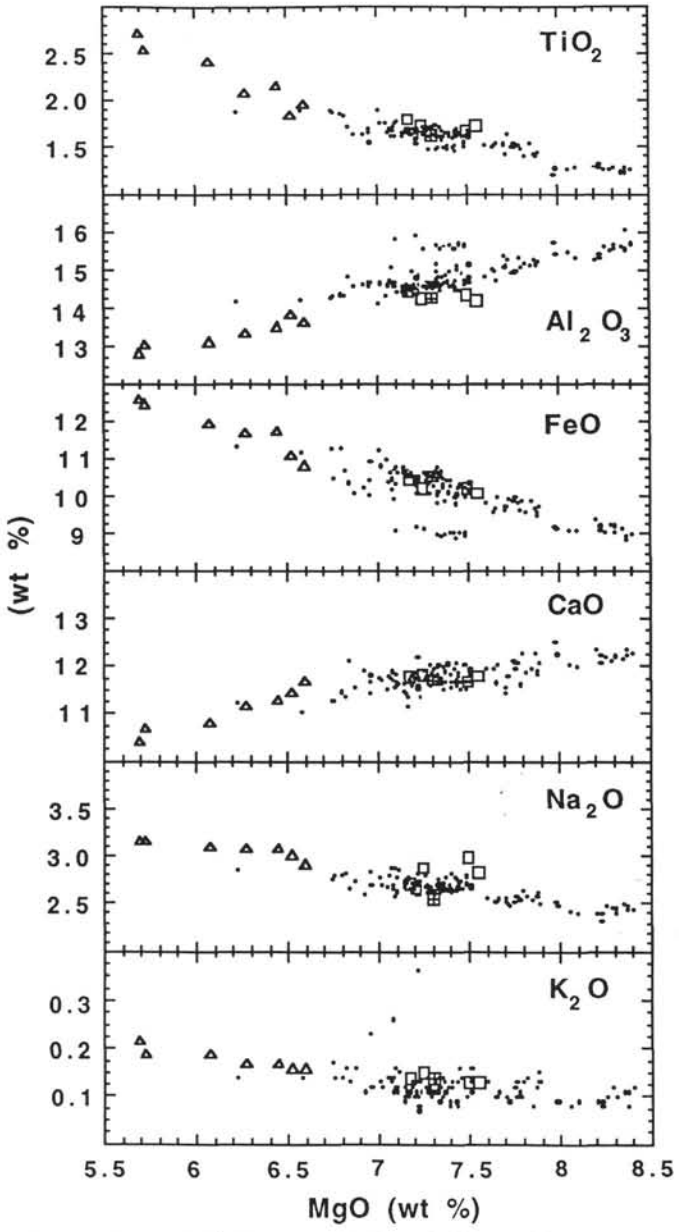

Figure 3. MgO variation diagrams with plots of 139 erupted lava compositions (Batiza and Niu, 1992) from the 9°30′N segment of the East Pacific Rise (dot), the initial Unit 1 basalt starting composition (square with cross), the compositions of experimental liquids in equilibrium with olivine ± plagioclase (empty square), and olivine-plagioclase-clinopyroxene (triangle).

Additional support for this conclusion can be found in Figure 7, which shows a CaO-MgO variation diagram on which are plotted the olivine-plagioclase-augite-saturated experimental liquids along with all of the EPR lava analyses from Batiza and Niu (1992). The solid line represents a linear regression through the lava data set. The lower right section of the figure shows the predicted slopes for typical liquid lines of descent calculated for olivine-plagioclase-clinopyroxene crystallization at 0.001, 2, and 8 kb. These trends are calculated following the procedure of Grove et al. (1992) and assume a parental magma equivalent in composition to the most MgO-rich EPR lava reported by Batiza and Niu (1992). The predicted effect of increasing fractionation pressure is to decrease the slope of the CaO-MgO variation. The overall trend of the EPR lavas is less steep than the 1-atm

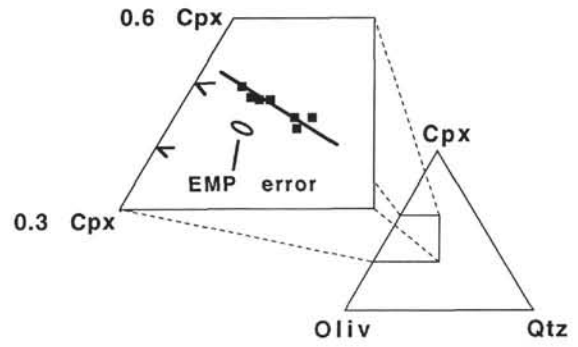

Figure 4. Pseudo-ternary olivine-clinopyroxene-quartz diagram showing projected positions of all oliv-plag-cpx-saturated experimental liquids (after Walker et al., 1979). The solid line indicates the inferred position of the 1-atm olivine-plagioclase-clinopyroxene-liquid cotectic boundary curve. The EMP error ellipse represents the standard deviation of the mean (2 sigma) of 10 replicate glass analyses from the highest temperature (1190°C) experiment (142-QFM-3).

trend defined by the experimental liquids. Therefore, this observation is consistent with fractionation at elevated pressures as predicted earlier from the pseudo-ternary phase diagrams. A rough estimate of the pressure range over which fractionation occurred can be made by comparing the slopes of the best-fit line in Figure 7 ($m = 0.46 \pm 0.8$) with the calculated CaO-MgO slopes for fractionation at different pressures. In Figure 8, the three calculated slopes from Figure 6 (P = 0.001, 2, 8 kb) are plotted against pressure along with a best-fit exponential curve ($r = 0.99$). Figure 8 also shows the observed CaO-MgO slope for the EPR lavas, which predicts a fractional crystallization pressure somewhere between 1.9 and 3.9 kb.

The nearly 2 kb uncertainty associated with this estimate of fractionation pressure is quite large, and a further refinement of the fractionation pressure is desirable. Given that the starting lava (or liquid) composition employed in this study is thought to be the result of fractional crystallization of olivine, plagioclase, and clinopyroxene, a potentially useful technique for estimating the pressure at which the fractionation actually occurred would be to determine that pressure at which the experimental liquidus of the starting composition is multiply saturated with all three solid phases (e.g., Bender et al., 1978; Fisk et al., 1980). Provided that the fractionation pressure at which the starting liquid composition was generated is the same pressure as that at which the entire EPR lava suite was generated, such information could help further constrain the rather large pressure estimate arrived at above. In Figure 9, the 1-atm liquidus temperatures of olivine, plagioclase, and clinopyroxene determined in this study have been combined with estimated values for the slopes of the corresponding liquidus boundaries in P-T space (dT/dP, °C/kb) to generate a synthetic pressure-temperature phase diagram for the starting composition used in this study (e.g., Fisk et al., 1980). The liquidus boundary slopes used in constructing Figure 9 are olivine (1.6°C/kb)), plagioclase (4.3°C/kb), and clinopyroxene (9.9°C/kb). These values represent the average liquidus boundary slopes based on three different experimental studies of tholeiitic basalts similar in composition to the starting basalt used here (Thompson, 1972; Fuji and Kushiro, 1977; Grove et al., 1990). Figure 8 shows that the olivine, plagioclase, and clinopyroxene liquidus boundaries converge at a pressure of 1.9 kb. If the ± 2.5°C uncertainty in the liquidus boundaries themselves is taken into account, this liquidus boundary convergence pressure lies somewhere between 1.5 and 2.3 kb. This represents the pressure at which the starting composition's liquidus boundary could be multiply saturated with olivine, plagioclase, and clinopyroxene and, therefore, the pressure at which the same starting composition could have been generated by fractional crystallization. If it is assumed that the starting liquid composition was generated at

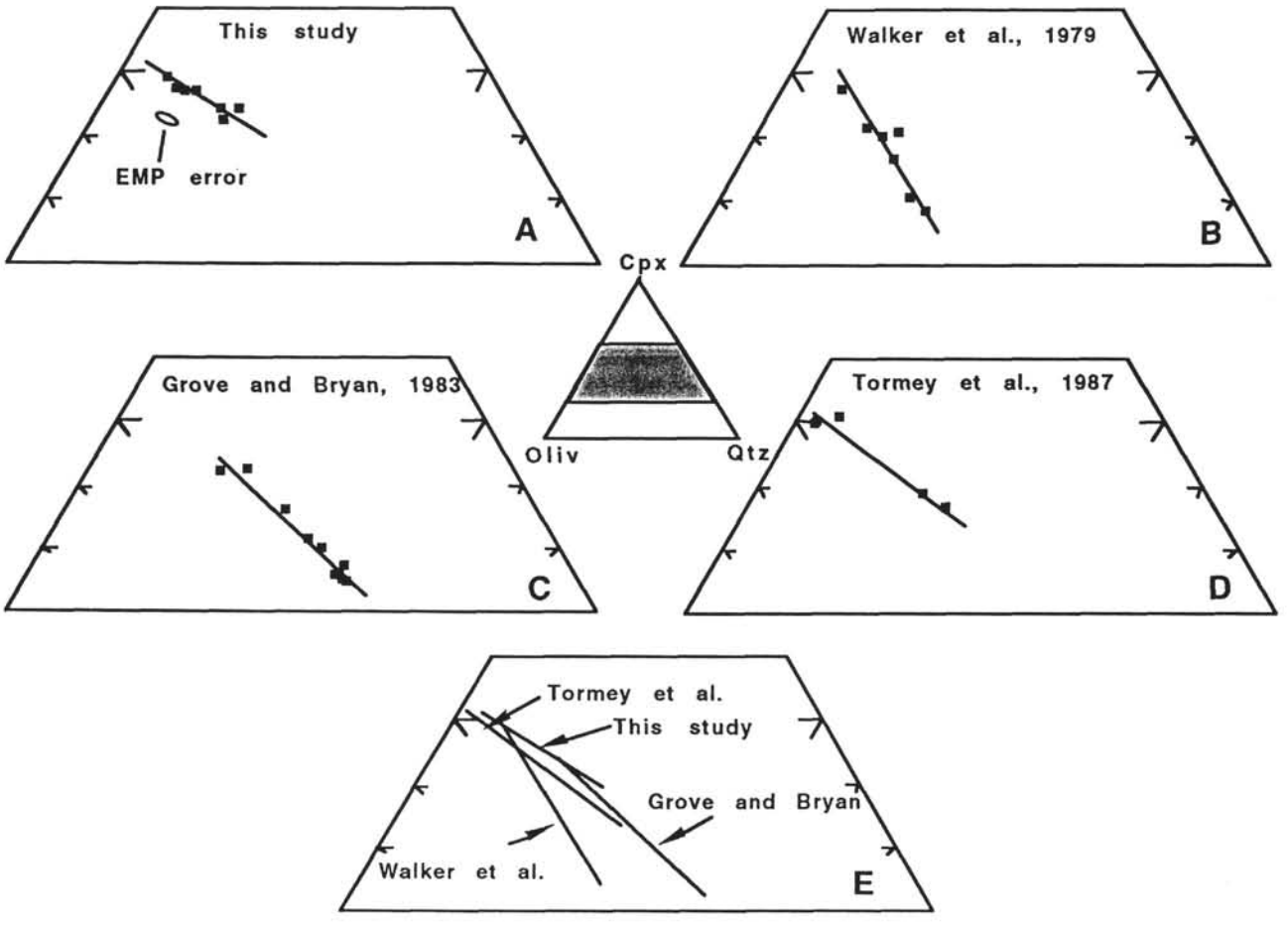

Figure 5. Comparison of experimentally determined olivine-plagioclase-clinopyroxene-liquid cotectic boundary curves as projected in the olivine-clinopyroxene-quartz pseudo-ternary (after Walker et al., 1979) from this study and previous experimental studies on mid-ocean ridge starting compositions (Walker et al., 1979; Grove and Bryan, 1983; Tormey et al., 1987).

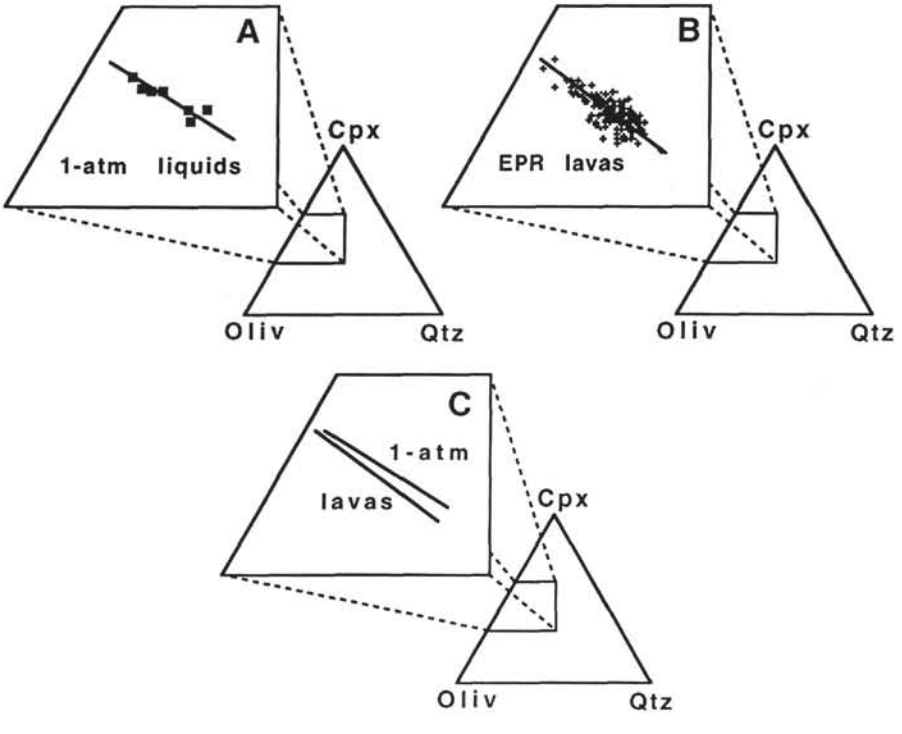

Figure 6. Pseudo-ternary olivine-clinopyroxene-quartz diagrams (after Walker et al., 1979) showing: **A,** the projected positions of all olivine-plagioclase-clinopyroxene-saturated experimental liquids from this study and the inferred location of the 1-atm olivine-plagioclase-clinopyroxene-liquid cotectic boundary curve; **B,** the projected positions of 139 lava analyses from the 9°30′N segment of the EPR (from Batiza and Niu, 1992) and a best-fit line indicating the overall trend of the lava data set; and **C,** a comparison of the 1-atm cotectic boundary curve and t<he trend of the lava data set. Note that the natural lavas define a trend that is parallel to the 1-atm boundary curve but slightly offset in the olivine-rich (i.e., higher pressure) direction.

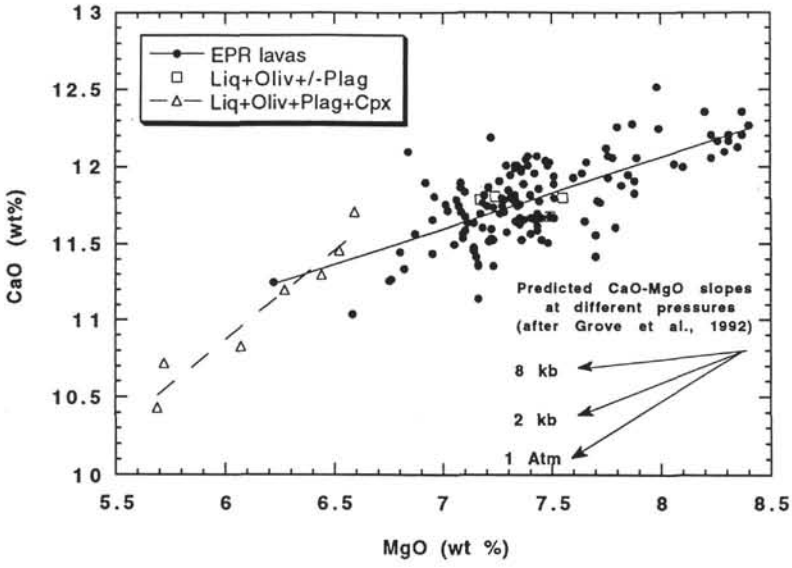

Figure 7. CaO-MgO variation diagram showing all the compositions of experimental liquids saturated with olivine ± plagioclase and olivine-plagioclase-clinopyroxene as well as 139 natural lava analyses (Batiza and Niu, 1992) from the 9°30′N segment of the EPR. The solid line shows the results of a linear regression through the EPR lava data and has a slope of 0.46 ± 0.8 (2-sigma confidence level). The dashed line shows the results of a linear regression through the olivine-plagioclase-clinopyroxene-saturated experimental liquids. Also shown are the calculated slopes for typical liquid lines of descent at 0.001, 2, and 8 kb (after Grove et al., 1992). Increased pressure leads to a decrease in the slope of the CaO-MgO variation. The lavas define a CaO-MgO variation less steep than that defined by the 1-atm experiments, indicating fractionation at elevated pressures.

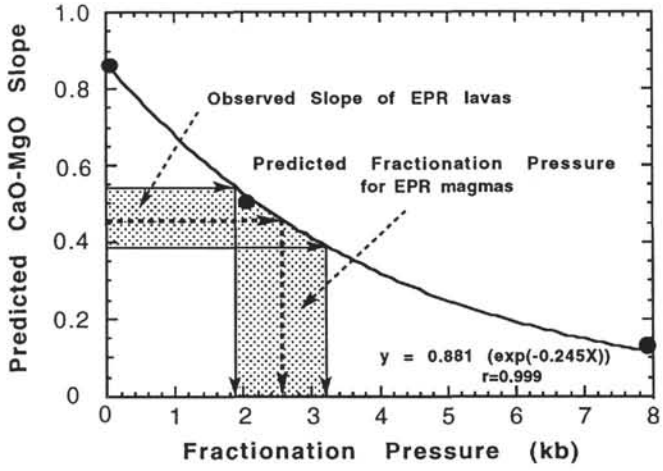

Figure 8. Calculated CaO-MgO variation slopes from Figure 7 vs. crystallization pressure (after Grove et al., 1992). The curve through the three data points is a best-fit exponential curve ($r = 0.999$) that shows the likely relationship between crystallization pressure and the slope of the resultant CaO-MgO variation. Also indicated is the observed slope of the EPR lava data set ($m = 0.46 \pm 0.8$). The observed slope predicts that fractionation of the EPR magmas occurred at a pressure somewhere between 1.9 and 3.1 kb.

the same pressure as the rest of the EPR lava suite, then these results suggest a general fractionation pressure beneath the EPR of about 1.9 ± 0.4 kb.

DISCUSSION

Estimated Fractionation Pressure and the Location of Fractional Crystallization Processes

Based on a good agreement between the projected positions of their EPR lava data with the projected position of the Walker et al. (1979) 1-atm cotectic boundary curve in the olivine-clinopyroxene-quartz pseudo-ternary diagram, Batiza and Niu (1992) concluded that the complete spectrum of erupted lava compositions could be generated by fractional crystallization within the axial magma chamber at very low-pressures ($P < 1$ kb). In contrast, the present study, based on experimental results from a genetically related basalt starting composition, suggests that fractional crystallization occurred at somewhat elevated pressures of about 2 kb. Elevated-pressure fractionation has been inferred beneath nearby segments of the EPR between 10° and 12°N (Thompson et al., 1989; Grove et al., 1992) and now appears to be an important attribute of fast-spreading mid-ocean ridge magmatic systems.

The predicted fractionation pressure of about 1.9 ± 0.4 kb has significant implications for the location and nature of fractional crystallization processes beneath the EPR. Figure 10 shows a calculated pressure-depth curve for the region beneath the EPR at 9°30′N based on the density model of Vera et al. (1990). Given their inferred location of the axial magma chamber at a depth of 1.4 to 2.2 km below the seafloor, predicted pressures within the chamber range from about 0.7 to 0.9 kb. This value is significantly lower than the 1.9 ± 0.4 kb pressure predicted for fractionation beneath this segment of the EPR, suggesting that all fractional crystallization occurred *beneath* rather than within the axial magma chamber. Figure 10 also shows that a fractionation pressure of 1.9 ± 0.4 kb could place olivine-plagioclase-clinopyroxene fractionation either above or below the crust-mantle boundary. Given that the fractionation process itself necessarily generates rocks of gabbroic composition (olivine, plagioclase, clinopyroxene), it seems most likely that fractionation actually took place within the crust above the crust-mantle boundary. If correct, the predicted fractionation pressure suggests that the bulk of the fractionation occurred within the lower portion of the crust rather than the region directly beneath the axial magma chamber, though fractionation within the mid- to upper-crust cannot be ruled out entirely.

Fractional Crystallization Pressure and the Nature of Fractional Crystallization Processes

The results of this study suggest that most (if not all) fractionation occurs within the lower crust well beneath the axial magma chamber, raising important questions regarding the overall nature of fractional crystallization processes beneath fast-spreading mid-ocean ridge systems such as the EPR. Traditionally, fractional crystallization has been viewed as a process that occurs through either gravitational crystal settling or sidewall/bottom floor crystallization and convective fractionation (e.g., Sparks et al., 1984). A fundamental requirement for either of these two mechanisms is the presence of a magma body. If the lower crustal region beneath the EPR does indeed consist of a crystal-rich mush zone as suggested by Sinton and Detrick (1992), then neither of these mechanisms is viable unless the mush zone itself contains individual bodies of magma as has been suggest-

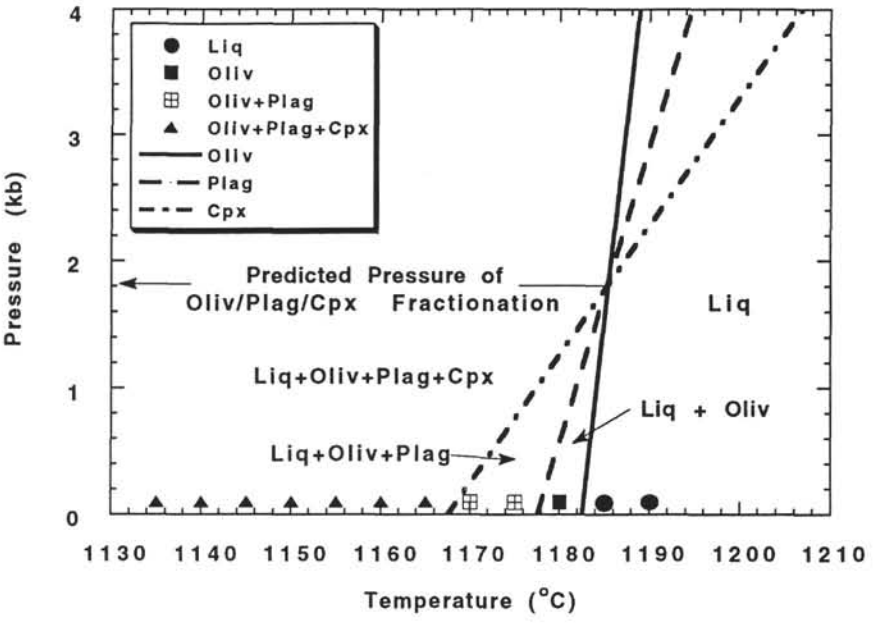

Figure 9. Synthetic pressure-temperature phase diagram for the 142-864A-1M starting basalt used in this study. The 1-atm crystallization temperatures of olivine, plagioclase, and clinopyroxene have been extended to higher pressures assuming pressure corrections for crystallization temperatures (dT/dP) of 1.6°C/kb (olivine), 4.3°C/kb (plagioclase), and 9.9°C/kb (clinopyroxene). These values are based on the average of three high-pressure experimental studies performed on tholeiitic basalts with compositions similar to the present starting basalt (Thompson, 1972; Fuji and Kushiro, 1977; Grove et al., 1990). Note that the predicted olivine, plagioclase, and clinopyroxene liquidus boundaries converge at a pressure of 1.9 kb, implying that a magma represented by the basalt starting composition could have been generated by combined olivine, plagioclase, and clinopyroxene fractionation at this same pressure.

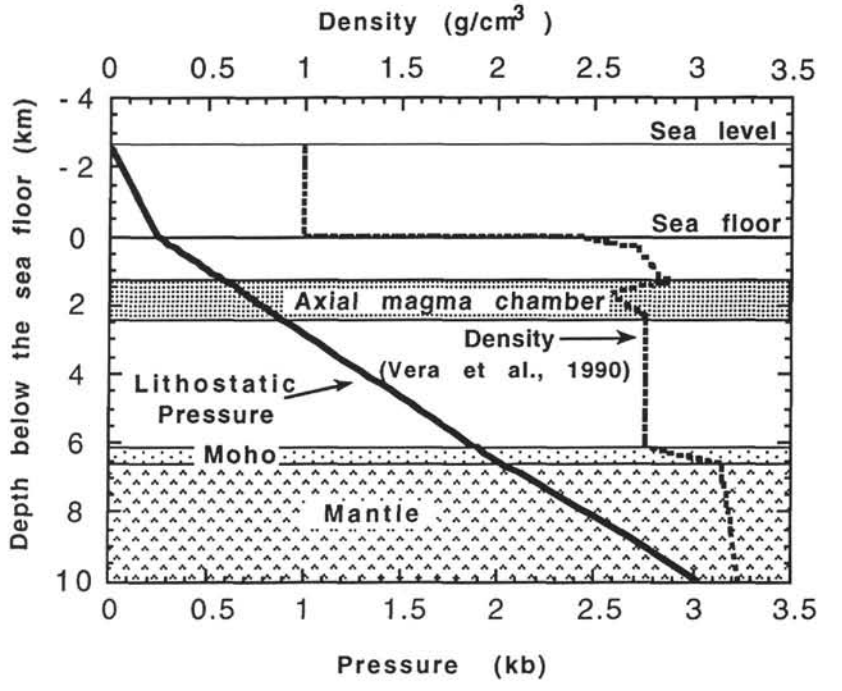

Figure 10. Calculated lithospheric pressure gradient beneath the EPR at 9°30′N based on the crustal density/structure model of Vera et al. (1990). Note that an inferred fractional crystallization pressure of around 1.9 kb places the fractionation at or near the base of the crust.

ed elsewhere for slow-spreading ridge systems (e.g., Sinton and Detrick, 1992; Grove et al., 1992). The present study cannot address this possibility. However, a parallel study of major, minor and trace element zonation patterns in plagioclase phenocrysts from the same EPR basalt used presently as a starting composition (Brophy and Allan, 1993) suggests that the mush zone is indeed characterized by small bodies of magma, but bodies that are sufficiently short lived (on the order of years) that appreciable fractionation through traditional mechanisms such as crystal settling or convective fractionation is unlikely. Brophy and Allan (1993) have suggested a possible alternative wherein buoyancy-driven melts migrate upwards through the mush zone, all the while interacting (i.e., fractionating) with the crystalline material through which they pass (a potential form of in-situ crystallization). At some point, the upward migrating melts coalesce to form small pockets or bodies of magma which move upward and ultimately pass through the bottom of the axial magma chamber. Whether or not a similar process can be inferred beneath slow-spreading ridge systems remains to be seen.

CONCLUSIONS

A series of 1-atm phase equilibrium experiments were conducted on a moderately evolved N-MORB sampled during drilling of the East Pacific Rise (EPR) ridge crest at 9°30′N. Comparison through different techniques of the experimental liquid compositions with the compositions of natural lavas erupted along the same area of the EPR suggests an origin through fractional crystallization at a pressure of

about 1.9 ± 0.4 kb. This places fractional crystallization well beneath the axial magma chamber and within the lower crust. This finding all but rules out the possibility of significant amounts of fractional crystallization within the low-pressure axial magma chamber beneath this (and other?) segments of the EPR, as well as other fast-spreading ridge systems. Given that little to no fractional crystallization occurs within the axial magma chamber, it is suggested that fractional crystallization occurs during upward melt migration as rising melts pass through and interact with solid and partially crystalline material in the roots of the magmatic system.

ACKNOWLEDGMENTS

I wish to thank Dana Johnston for permitting me to conduct the experiments in his laboratory as well as for badly needed instruction on experimental design and technique. This paper has benefited significantly from a review by Ro Kinzler. This work was supported by a grant from USSAC through the Texas A&M Research Foundation to J. Brophy.

REFERENCES*

Batiza, R., and Niu, Y., 1992. Petrology and magma chamber processes at the East Pacific Rise ~9°30′N. *J. Geophys. Res.*, 97:6779–6797.

Bender, J.F., Hodges, F.N., and Bence, A.E., 1978. Petrogenesis of basalts from the Project FAMOUS area: experimental study from 0 to 15 kbars. *Earth Planet. Sci. Lett.*, 41:277–302.

Brophy, J.G., and Allan, J.F., 1993. Textural and mineralogic studies of plagioclase phenocrysts from ODP Leg 142, Site 864A: Implications for magmatic processes beneath the East Pacific Rise (EPR), 9°30′N. *Eos*, 74:644.

Bryan, W.B., and Moore, J.G., 1977. Compositional variations of young basalts in the Mid-Atlantic Ridge rift valley near latitude 36°49′N. *Geol. Soc. Am. Bull.*, 88:556–570.

Fisk, M.R., Schilling, J.G., and Sigurdsson, H., 1980. An experimental investigation of Iceland and Reykjanes Ridge tholeiites: I. Phase relations. *Contrib. Mineral. Petrol.*, 74:361–374.

Fujii, T., and Kushiro, I., 1977. Melting relations and viscosity of an abyssal tholeiite. *Yearbook—Carnegie Inst. Washington*, 76:461–465.

Grove, T.L., and Bryan, W.B., 1983. Fractionation of pyroxene-phyric MORB at low pressure: an experimental study. *Contrib. Mineral. Petrol.*, 84:293–309.

Grove, T.L., Kinzler, R.J., and Bryan, W.B., 1990. Natural and experimental phase relations of lavas from Serocki volcano. *In* Detrick, R., Honnorez, J., Bryan, W.B., Juteau, T., et al., *Proc. ODP, Sci. Results*, 106/109: College Station, TX (Ocean Drilling Program), 9–17.

————, 1992. Fractionation of mid-ocean ridge basalt (MORB). *In* Morgan, J.P., Blackman, D.K., and Sinton, J.M. (Eds.), *Mantle Flow and Melt Generation at Mid-Ocean Ridges*. Geophys. Monogr., Am. Geophys. Union, 71:281–310.

Langmuir, C.H., Bender, J.F., and Batiza, R., 1986. Petrologic and tectonic segmentation of the East Pacific Rise, 5°30′–14°30′. *Nature*, 322:422–429.

Pallister, J.S., and Hopson, C.A., 1981. Samail ophiolite plutonic suite: field relations, phase variation, cryptic variation and layering, and a model of a spreading ridge magma chamber. *J. Geophys. Res.*, 86:2593–2644.

Reynolds, J.R., Langmuir, C.H., Bender, J.F., Kastens, K.A., and Bryan, W.B.F., 1992. Spatial and temporal variability in the geochemistry of basalts from the East Pacific Rise. *Nature*, 359:493–499.

Sinton, J.M., and Detrick, R.S., 1992. Mid-ocean ridge magma chambers. *J. Geophys. Res.*, 97:197–216.

Sparks, R.S.J., Huppert, H.E., and Turner, J.S., 1984. The fluid dynamics of evolving magma chambers. *Philos. Trans. R. Soc. London A*, 310:511–534.

Stolper, E., 1980. A phase diagram for mid-ocean ridge basalts: preliminary results and implications for petrogenesis. *Contrib. Mineral. Petrol.*, 78:13–27.

Thompson, G., Bryan, W.B. and Humphris, S.E., 1989. Axial volcanism on the East Pacific Rise, 10–12°N. *In* Saunders, A.D., and Norry, M.J. (Eds.), *Magmatism in the Ocean Basins*. Geol. Soc. Spec. Publ. London, 42:181–200.

Thompson, R.N., 1972. Melting behavior of two Snake River lavas at pressures up to 35 kb. *Yearbook—Carnegie Inst. Washington*, 71:406–410.

Tormey, D.R., Grove, T.L., and Bryan, W.B., 1987. Experimental petrology of normal MORB near the Kane Fracture Zone: 22°–25°N, Mid Atlantic Ridge. *Contrib. Mineral. Petrol.*, 96:121–139.

Vera, E.E., Mutter, J.C., Buhl, P., Orcutt, J.A., Harding, A.J., Kappus, M.E., Detrick, R.S., and Brocher, T.M., 1990. The structure of 0- to 0.2-m.y.-old oceanic crust at 9°N on the East Pacific Rise from expanded spread profiles. *J. Geophys. Res.*, 95:15529–15556.

Walker, D., Shibata, T., and Delong, S.E., 1979. Abyssal tholeiites from the Oceanographer Fracture Zone, II: Phase equilibria and mixing. *Contrib. Mineral. Petrol.*, 70:111–125.

Date of initial receipt: 30 August 1993
Date of acceptance: 10 June 1994
Ms 142SR-104

*Abbreviations for names of organizations and publications in ODP reference lists follow the style given in *Chemical Abstracts Service Source Index* (published by American Chemical Society).